Physica A 526 (2019) 120990

Contents lists available at ScienceDirect

Physica A

journal homepage: www.elsevier.com/locate/physa

Stability analysis of an improved car-following model accounting for the driver's characteristics and automation

Hongzhuan Zhao [a], Qiguang Chen [b,*], Wei Shi [c], Tianlong Gu [d], Wenyong Li [a]

[a] School of Architecture and Transportation Engineering, Guilin University of Electronic Technology, Guilin 541004, Guangxi, PR China
[b] Guangxi University of Chinese Medicine Pharmaceutical Factory, Guangxi University of Chinese Medicine, Nanning 530000, Guangxi, PR China
[c] School of Electronics and Information Engineering, Wuzhou University, Wuzhou 543002, Guangxi, PR China
[d] School of Information and Communication, Guilin University of Electronic Technology, Guilin 541004, Guangxi, PR China

HIGHLIGHTS

- This paper presents car-following model with combined mode between driver's characteristics and automation.
- This paper attempts to reveal the intrinsic features of driving.
- Stability analysis is performed by adopting frequency domain sweeping method.

ARTICLE INFO

Article history:
Received 14 June 2018
Received in revised form 22 January 2019
Available online 10 April 2019

Keywords:
Car-following model
Stability analysis
Driver's characteristics
Aggressiveness
Automation

ABSTRACT

This study presents an improved car-following model accounting for the driver's characteristics and automation for longitudinal driving. We attempt to reveal some features of driving behavior, which drivers make decision in consideration with delayed decision and aggressiveness as well as the automated controller. The delayed decision and aggressiveness of drivers are represented via the integral term with kernel function and headway perturbation, and the automated controller consists of proportional–derivative element. Stability analysis is performed both driver's characteristics and controller gains adopting frequency domain sweeping method. Stability regions of proposed model show the relationships between driver's characteristics and automated controller. Some numerical examples are given to illustrate the effectiveness of the proposed methods and interpret the relation between driver's characteristics and automated controller.

1. Introduction

Traffic accidents remain a common cause of death and disability, which approximately 90% of the cases are concerned with the drivers [1]. The accidents may be attributed to degradation of drivers' performance caused by such factors as fatigue, drowsiness, or inattention. This fact has motivated major research effort aimed at helping drivers and improving safety, especially via the use of active safety systems.

The present scientific and technical advancements offer the guarantees to develop Advanced Driver Assistance Systems(ADAS). ADAS can assist the driver to safely drive the vehicle, which reduces work load of driving and road accidents [2–4]. Soualmi et al. [2] classified driver assistance systems into three groups. For first group, the systems

* Corresponding author.
E-mail address: chenqiguang2008@163.com (Q. Chen).

https://doi.org/10.1016/j.physa.2019.04.226
0378-4371/

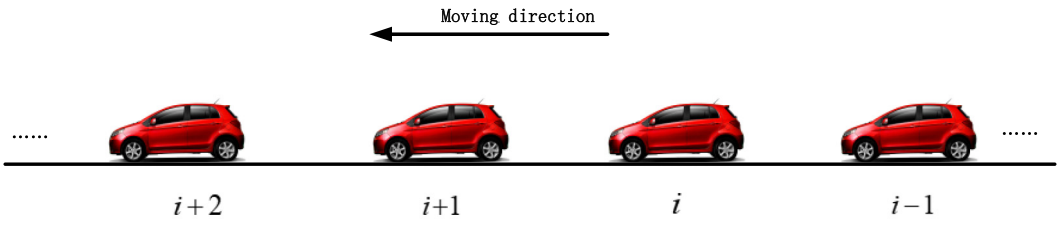

Fig. 1. The platoon of vehicles.

try to stabilize the vehicle by acting at a low control level so that the vehicle remains more stable and is controllable by the driver, *e.g.* ABS and ESP. The common feature of such systems is their restriction to get information only on the vehicle's state. For second group, the systems alert the driver when a risk is detected, *e.g.* LDWS(Lane Departure Warning Systems) [3], which no action is being taken to avoid the hazards. These systems can be hard to play critical role when the driver is inattentive, even exclude the driver in the driving process [4]. For third group, the systems can take actions and control the vehicle's dynamics and trajectory which perform a part of the driving task, like ACC/CACC for longitudinal control [5,6].

With regards to driver-automation interaction viewpoint, longitudinal control of vehicle with the driver and automated controllers involves the crucial study of the interaction between two agents. Shared control [7,8] was introduced as a guideline for driver assistance system concept. The interactions between the driver and his/her vehicle via the system are incorporated in the same manner as those between the rider and his/her horse through the controls [8]. The states of the system are taken into account of processing the information provided by driver state, vehicle state and traffic conditions [9–11]. Depending on the state of each component, the decisions are taken to choose the mode: manual mode, full automatic mode, or combined mode.

In order to stabilize traffic flow and enhance driving safety, the study of longitudinal driving along these main lines has direct connections to developing traffic control strategies by constructing decentralized control [12–14], adaptive control [15], nonlinear control [16,17], and gain scheduling techniques [18]. The above mentioned contributions are classified into three categories [19,20]: (i) investigating how the headway perturbations dynamics propagates upstream of traffic flow; (ii) proposing the analysis method to reveal natural characteristics of traffic dynamics under perturbations; (iii) designing appropriate controllers to suppress amplification of perturbations. It is important to note that there exist various complex instability mechanisms in traffic flow investigated by linear and nonlinear analysis. Seiler et al. [21] analyzed disturbance propagation in a platoon and showed error amplification of intra-platoon spacing under a predecessor-following control strategy, in which each vehicle only has the relative position to its preceding one. To maintain constant intra-platoon spacing, a predecessor-leader control strategy [22] was proposed wherein each vehicle is supposed to get information from both its preceding vehicle and the platoon leader. In [23], platoon stability was investigated under both predecessor-following and symmetric bidirectional communication structures with linear and nonlinear controllers, respectively. Above-mentioned contributions investigate stability of platoon considering all vehicles are full automatic or manual. In fact, however, the driving behaviors are a cooperative decision-making under the interaction of driver and ADAS.

Traffic instabilities describe terrible traffic phenomena, such as oscillations, traffic waves, stop-and-go traffic and the like. Stability analysis of traffic flow attracts the attention of researchers [24]. The methods of linear stability analysis consider that a small perturbation of steady state will propagate with time [25–31]. For larger perturbations, nonlinear effect of traffic flow need characterize wave profiles. The nonlinear equations of traffic flow could derive the nonlinear characteristics [32–35], such as solitary waves, kink waves and triangular waves. Based on microscopic traffic models and its extended models, many researchers investigated various properties of the traffic flow [36–44].

In this paper, the starting point in our study is a type of car-following mode, e.g. Pipes model [45], represented by a set of differential equations which drivers drive at desired velocity and desired gap in a single lane without changing lanes and overtaking (Fig. 1). Adopting this mode, we attempt to reveal the intrinsic features, where drivers make decisions in consideration with memory and aggressiveness as well as the automated controller works in parallel to compensate the inter-vehicle gaps. Our focus is mainly on the effects of driver's characteristics and automated controllers which attempts to capture new information that can be useful in designing controller gains.

This paper is organized as follows. Section 2 introduces dynamics model and its interest in the control of nonlinear systems. Section 3 analyzes stability of the proposed model using frequency domain method. Driver's characteristics are revealed and correspondence relationships are obtained via investigating aggressiveness and delays in Section 4. Section 5 concludes the results of this work and gives a guideline of future works.

2. Model

Some interesting and meaningful mathematical models and the relevant works are investigated by many scholars, which focus on the behavior of a vehicle group which consists of vehicles running on a single road without overtaking

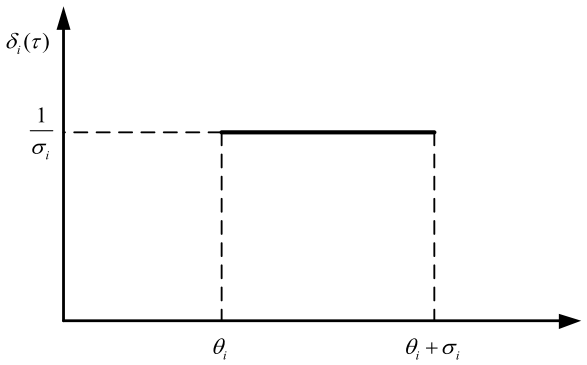

Fig. 2. Uniform distribution suited to depict the short-term memory effect of decision process.

shown in Fig. 1. Mathematical model of vehicle group can be expressed as nonlinear dynamic systems of the form

$$\frac{dv_i(t)}{dt} = f(h_i(t-\tau), \dot{h}_i(t-\sigma), v_i(t-\kappa)), \tag{1}$$

where x_i is the position of the ith vehicle, v_i is the velocity of the ith vehicle. Headway distance $h_i = x_{i+1}(t) - x_i(t)$, velocity difference $\dot{h}_i = v_{i+1}(t) - v_i(t)$. The acceleration has to be given as the nonlinear function of stimuli that are usually the headway distance h_i, the velocity difference $\dot{h}_i$ and the vehicle's own velocity v_i. Where τ, σ, κ represent driver reaction delays to different stimuli. To make the model more tractable, simple relations may be assumed between the different delays. The terms with delays on the right-hand side of model (1) derive from the driver.

Linearizing model (1) around an equilibrium configuration of traffic flow, we have

$$h_i(t) \equiv h^*, \dot{h}_i \equiv 0, v_i(t) \equiv v^*, \tag{2}$$

The linearization of model (1) based on form (2) can be carried out to analyze the dynamics of the small perturbations. Defining the perturbations $\widetilde{h}_i = h_i(t) - h^*$, $\widetilde{v}_i = v_i(t) - v^*$. Dynamics function are simplified forms of model (1) describing the acceleration perturbations as a function of velocity and position perturbations. We can represent the dynamics with the linear delay differential equation

$$\dot{\widetilde{v}}_i(t) = A\widetilde{h}_i(t-\tau) + B\dot{\widetilde{h}}_i(t-\sigma) - C\widetilde{v}_i(t-\kappa), \tag{3}$$

where the derivatives

$$A = \partial_h f(h^*, 0, v^*), B = \partial_{h'} f(h^*, 0, v^*), \text{ and } C = -\partial_v f(h^*, 0, v^*), \tag{4}$$

Set $\widetilde{v}_i(t) = \dot{y}_i(t)$, we rearrange Eq. (3) and obtain the linearized equations

$$\ddot{y}_i(t) = AH_i(t-\tau) + B\dot{H}_i(t-\sigma) - C\dot{y}_i(t-\kappa), \tag{5}$$

where $H_i(t) = y_{i+1}(t) - y_i(t)$ is headway perturbation between vehicles i and (i+1). The terms with$y_i(t)$ are the non-homogeneous parts of Eq. (5) and thus $i = 1, 2, \ldots, n-1$ with n being the number of vehicles. Eq. (5) formulates that the driver attempts to weaken the perturbed velocity and position errors using the gains A, B and C with the control objective of keeping constant velocity around.

We think considering driver and an automated controller with Eq. (5) is interesting and meaningful, which requires us to develop appropriate mathematical tools for stability analysis of the proposed model. Let us discuss the proposed model of driver behavior and how an automated controller is considered in our control problem. Driver's behavior includes the driver's aggressiveness and memory. Driver's memory effects in decision process can be modeled using particular distribution functions to depict the short term memory of driver. One of the simplest distribution functions is uniform function distribution inspired from Ref [20].

$$\delta_i(\tau) = \begin{cases} \dfrac{1}{\sigma_i}, & \theta_i \le \tau \le \theta_i + \sigma_i \\ 0, & \text{for else} \end{cases}, \tag{6}$$

where θ_i is the memory dead-time of ith driver, σ_i is memory window. The average of memory window is represented by (see Fig. 2).

$$\overline{\tau}_i = \theta_i + \frac{\sigma_i}{2}, \tag{7}$$

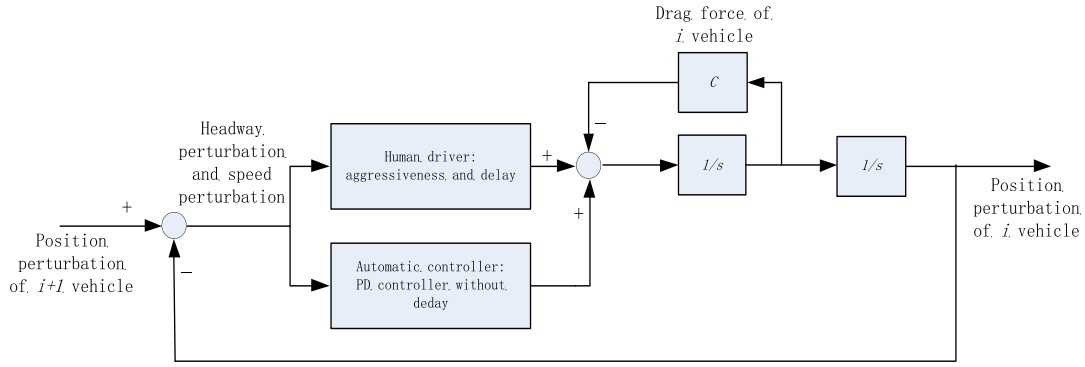

Fig. 3. Block scheme of proposed model between driver's characteristics and automation represented by integral–differential delay equation (8).

In light of the above discussions, we present the acceleration perturbations in the ith vehicle following the (i+1)th vehicle as

$$\begin{aligned}\ddot{y}_i(t) = {} & a_i \int_0^\infty \delta_i(\tau) H_i(t-\tau)d\tau + b_i \int_0^\infty \delta_i(\tau)\dot{H}_i(t-\tau)d\tau \\ & + K_{p,i}H_i(t) + K_{d,i}\dot{H}_i(t) - C_i\dot{y}_i(t)\end{aligned}, \tag{8}$$

where $K_{p,i}$ and $K_{d,i}$ are constant values that represent the proportional gain and derivative gain of the automated controller, respectively. The driver's decision is defined by the integral term of Eq. (8), which accounts for the weighted headway perturbation and perturbation of speed difference using the kernel function $\delta_i(\tau)$ that describe the driver's memory effect. The control block scheme of Eq. (8) is shown in Fig. 3.

3. Stability analysis

We analyze string stability of the proposed model in this section. Firstly, we start to identify the transfer function and characteristic equation of Eq. (8). Next, a frequency domain sweeping method is adapted to investigate stability conditions both the controller gain and driver's characteristics. Finally, some interesting phenomena of proposed model between driver's characteristics and automation are revealed.

3.1. The transfer function and characteristic equation

We consider proposed model between driver's characteristics and automation derived from traffic scenario is a linear homogeneous spatial configuration of the vehicles (Fig. 1). Therefore, we could pay close attention to string stability of two consecutive vehicles. To simplify the notation and without loss of generality, we denote $\delta_i(\tau) = \delta(\tau), \theta_i = \theta, \sigma_i = \sigma, K_{p,i} = K_p, K_{d,i} = K_d, C_i = C$ in Eq. (8). According to control theory, transfer function between two consecutive vehicles can be described by taking the Laplace transform of Eq. (8),

$$\begin{aligned}G(s) &= \frac{Y_i(s)}{Y_{i+1}(s)} = \frac{bs\Delta(s) + (K_d + C)s + K_p + a\Delta(s)}{s^2 + (b\Delta(s) + K_d + C)s + K_p + a\Delta(s)}, \\ \Delta(s) &= e^{-s\theta}\frac{1 - e^{-s\sigma}}{s\sigma}\end{aligned} \tag{9}$$

where $Y_i(s)$ and $Y_{i+1}(s)$ are Laplace transforms of the perturbations $y_i(t)$ and $y_{i+1}(t)$, respectively. $\Delta(s)$ is Laplace transforms of $\delta(\tau)$. The characteristic equation of Eq. (9) is the denominator of transfer function $G(s)$,

$$\Lambda(s) = s^2 + (b\Delta(s) + K_d + C)s + K_p + a\Delta(s), \tag{10}$$

Based on the characteristic Eq. (10), stability properties of the input–output system in Eq. (8) can be studied.

When $\sigma \to 0$, we know that $\delta(\tau) \to \infty$ and $\Delta(s) = 1$. In other words, the uniform distribution tends to Dirac distribution, and the characteristic equation is $\Lambda(s) = s^2 + (b + K_d + C)s + K_p + a$. Based on Routh stability criterion, the input–output system is asymptotically stable when the inequations. $b + K_d + C > 0$ and $K_p + a > 0$ are satisfied [20].

However, there are additional problems in the case that delay $\sigma \neq 0$. The two delay parameters θ, σ are independent, and delay σ exists as a coefficient of the characteristic equation, which is non-standard function. Meanwhile, we need also to discuss driver's aggressiveness.

Stability of Eq. (9) for a given set of parameters holds if and only if the characteristic roots of Eq. (10) all lie in the left half of the complex plane $\mathbb{C}$. The continuity of these roots with respect to the parameters can be shown to hold.

In order to solve the characteristic Eq. (10), we set $s = j\omega$, where $\omega \geq 0$. In other words, in order to obtain stability of input–output system (8), it is necessary to solve Eq. (11)

$$(j\omega)^2 + (be^{-j\omega\theta}\frac{1-e^{-j\omega\sigma}}{j\omega\sigma} + K_d + C)(j\omega) + K_p + ae^{-j\omega\theta}\frac{1-e^{-j\omega\sigma}}{j\omega\sigma} = 0, \tag{11}$$

It is worth mentioning that the particular structure of the problem we are dealing with ought to be treated as the controller gain parameter and driver's characteristics parameters independently.

Therefore, stability analysis of Eq. (9) is addressed via two patterns in this paper: (i) when the delay parameters and driver's aggressiveness are given, we will reveal stability features of the input–output system in the corresponding controller gain space; (ii) when controller gains K_d and K_p are given, we will study stability features in the corresponding delay parameters and driver aggressiveness.

3.2. Stability features in controller gain space

A parameter-sweeping approach is adapted to analyze the regions in the gain space (K_p, K_d), where the dynamics is characterized as stable or unstable. The boundaries parting stable from unstable regions need to be captured. The effort to achieve this requires explicit solutions. Assume that the delay parameter (θ, σ) is given, and frequency ω is a sweep parameter. Extract K_p and $K_d + C$ terms of controller gains in Eq. (11) on one side of the equation, and let the other side of the equation be denoted by the complex function $\Phi(\theta, \sigma, \omega)$, which can be computed for any sweep parameter $\omega \geq 0$. It is easy to express the controller gains as a function of ω,

$$K_p = P(\Phi(\theta, \sigma, \omega)), \tag{12}$$

and

$$K_d + C = \frac{D(\Phi(\theta, \sigma, \omega))}{\omega}, \tag{13}$$

Theorem 1. *The parameter $K_d + C$ found from Eq. (13) is bounded by $a\overline{\tau} - b$ for θ, σ and $\omega > 0$, when $\overline{\tau}$ is given.*

Proof. We analyze some algebraic operations and trigonometric functions,

$$\begin{aligned} &e^{-j\omega\theta}(1-e^{-j\omega\sigma}) = (\cos(\omega\theta) - j\sin(\omega\theta))(1-\cos(\omega\sigma) + j\sin(\omega\sigma)) \\ &= \cos(\omega\theta)(1-\cos(\omega\sigma)) + j\cos(\omega\theta)\sin(\omega\sigma) - j\sin(\omega\theta)(1-\cos(\omega\sigma)) \\ &-j^2\sin(\omega\theta)\sin(\omega\sigma) \\ &= \cos(\omega\theta)(1-\cos(\omega\sigma)) + \sin(\omega\theta)\sin(\omega\sigma) \\ &+j\cos(\omega\theta)\sin(\omega\sigma) - j\sin(\omega\theta)(1-\cos(\omega\sigma)) \end{aligned}, \tag{14}$$

According to Eq. (11), the imaginary part is extracted and one can show from Eq. (13) as follows

$$K_d + C = \frac{D(\Phi(\delta, \omega))}{\omega} = \frac{2a}{\omega^2\sigma}\sin(\omega\overline{\tau})\sin(\frac{\omega\sigma}{2}) - \frac{2b}{\omega\sigma}\cos(\omega\overline{\tau})\sin(\frac{\omega\sigma}{2}), \tag{15}$$

which is bounded by $a\overline{\tau} - b$ as $\omega \to 0^+$. This completes the proof.

The proof of Theorem 1 offers theoretic support about the boundaries that separate stability regions in the controller gain space. Except $\omega = 0$, we know that the points on stability boundaries cannot exceed the bound $a\overline{\tau} - b$ in $K_d + C$.

The controller gain K_p is acquired by similar analysis as follow

$$K_p = \omega^2 - \frac{2a}{\omega\sigma}\cos(\omega\overline{\tau})\sin(\frac{\omega\sigma}{2}) - \frac{2b}{\sigma}\sin(\omega\overline{\tau})\sin(\frac{\omega\sigma}{2}), \tag{16}$$

From Eq. (15), notice that K_p does not have an upper bound and it approaches to infinity when $\omega \to \infty$. Then, we discuss the specific circumstance when $\omega \to 0^+$.

Theorem 2. *The system expressed by Eq. (11) has an invariant root at $s = 0$ for $K_p = -a$, and double roots for $K_p = -a$ and $K_d + C = a\overline{\tau} - b$.*

Proof. As $s \to 0$ of Eq. (11), it is easy to obtain a solution $K_p = -a$ that is an invariant root.

Another way to think about Eq. (11), we turn into Eqs. (12) and (13). The limits are captured when $\omega \to 0$. So we obtain two roots $K_p = -a$ and $K_d + C = a\overline{\tau} - b$. This completes the proof.

Theorem 3. *The sensitivity of the invariant root $s = 0$ with respect to K_p is stability when $K_d + C > a\overline{\tau} - b$.*

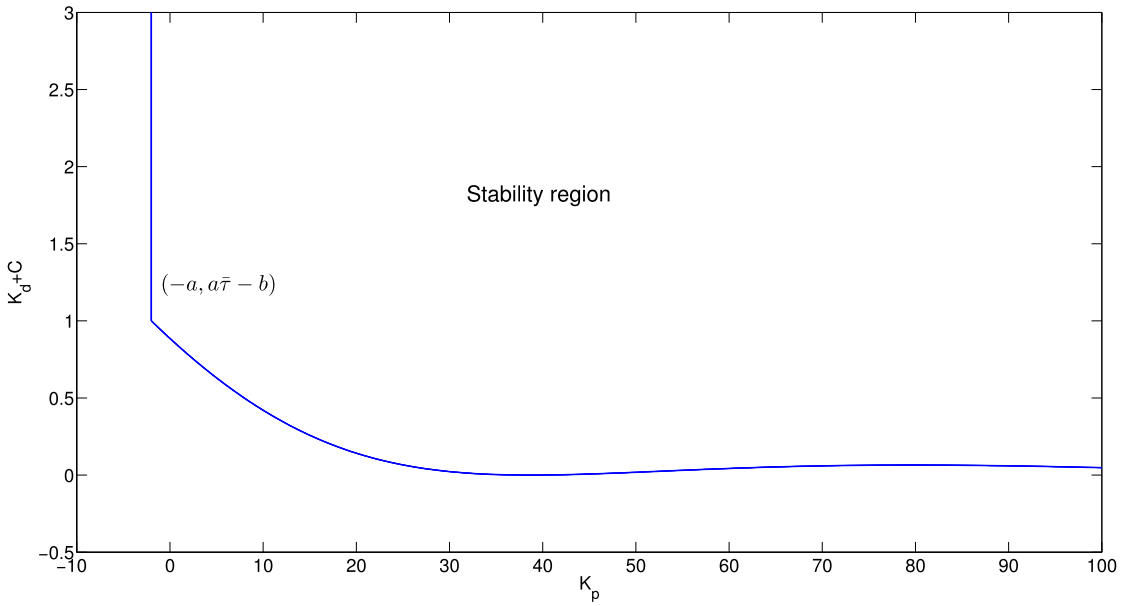

Fig. 4. The sufficient stability region for proposed model accounting for driver's characteristics and automation.

Proof. We use the implicit function theory on Λ in a small neighborhood around the origin of the complex plane, and express that

$$\frac{ds}{dK_p}|_{s\to 0^+} = -\frac{\partial s}{\partial \Lambda}\frac{\partial \Lambda}{\partial K_p}|_{s\to 0^+} = \frac{1}{(a\bar{\tau} - b) - (K_d + C)}, \tag{17}$$

We will obtain the root at s = 0 tends to move to $\mathbb{C}_-$ when $a\bar{\tau} - b < (K_d + C)$.

A rule arising from the above Theorem is that the root at $s = 0$ is stability when the coefficient $K_d + C$ is larger than $a\bar{\tau} - b$, including the driver aggressiveness a,b and $\bar{\tau} = \theta + \sigma/2$. This completes the proof.

Theorem 4. *Given $a\bar{\tau} - b = (K_d + C)$, input–output system (8) is asymptotically stable as $K_p > -a$.*

Proof. For sufficiently large $K_p^* > 0$ and $K_d^* + C > 0$ in Eq. (11), it is possible to enforce Eq. (10) to have no solutions for $\omega > 0$. This indicates that input–output system is stable for large gains independent of driver's aggressiveness and delay. Since $a\bar{\tau} - b$ is the bound of $K_d + C$ for all $\omega > 0$ and $K_d + C \to \infty$can occur only when $K_p \to -a$. It is easy to see that there is a continuous path in the $(K_p, K_d + C)$ parameter space without piercing through stability crossing curves. So, the point $(-a, a\bar{\tau} - b)$ can be chosen. This completes the proof.

In Fig. 4, the region corresponds to the sufficient stability conditions of proposed model between driver's characteristics and automation system for representative values of a, b and $\bar{\tau}$. Some numerical parameters are derived from reference [28], where $\theta = 0.1, \sigma = 1, a = 2, b = 0.2$ are taken.

3.3. Sufficient conditions of stability on controller gains

Theorem 5. *The proposed model between driver's characteristics and automation defined by transfer Eq. (9) is stable independent of delay if three conditions are held simultaneously as follows:*

(i) $K_d + C + b > 0, K_p + a > 0,$
(ii) $K_p^2 - a^2 \geq 0,$
(iii) $[4K_p + b^2 - (K_d + C)^2][(K_d + C)^2 - b^2) > 4a^2$ *whenever* $(K_d + C)^2 - b^2 - 2K_p < 0$

Proof. Conditions (i) guarantees stability of the delay-free system ($\tau = 0$). Otherwise, this system does not exhibit any $s = j\omega$ solutions and it guarantees that the system maintains its stability. Eq. (11) could be divided into two parts, as following,

$$K_p - \omega^2 + (K_d + C)(j\omega) = -(bj\omega + a)e^{-j\omega\theta}\frac{1 - e^{-j\omega\sigma}}{j\omega\sigma}, \tag{18}$$

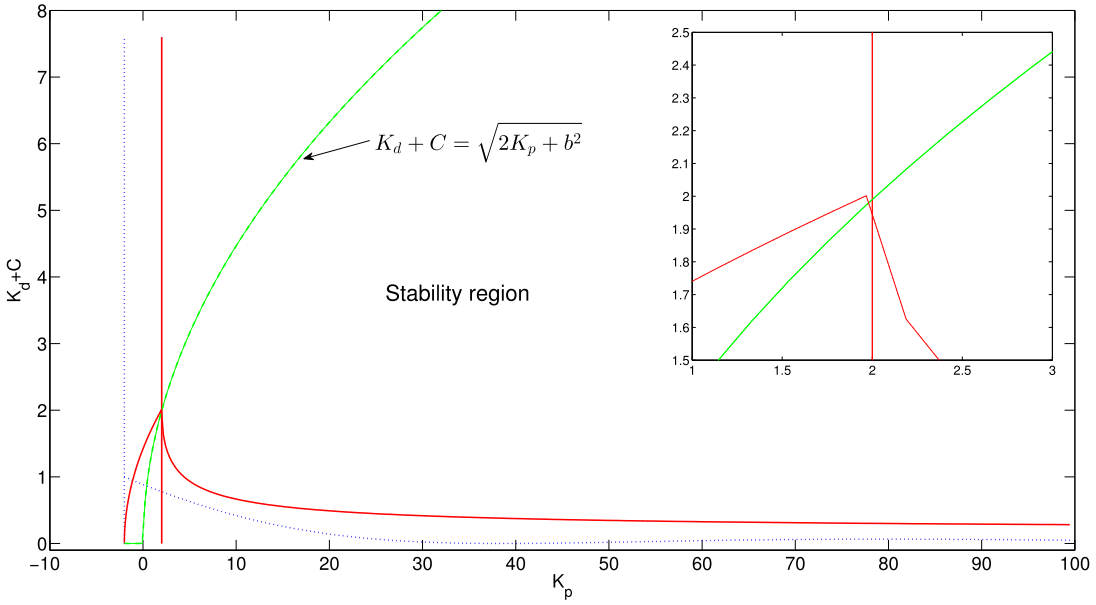

Fig. 5. The sufficient stability conditions of Theorems 5 and 6 Surrounded by green solid curve and red solid curves.

The left of Eq. (18) is $(K_p - \omega^2)^2 + \omega^2(K_d + C)^2$. The right of Eq. (18) is bounded

$$\left\|(bj\omega + a)e^{-j\omega\theta}\frac{1 - e^{-j\omega\sigma}}{j\omega\sigma}\right\|^2 = (a^2 + (b\omega)^2)\frac{2[1 - \cos(\omega\sigma)]}{(\omega\sigma)^2} \leq a^2 + (b\omega)^2, \tag{19}$$

It is sufficient that $(K_p - \omega^2)^2 + \omega^2(K_d + C)^2 > a^2 + (b\omega)^2$ so that there does not exist ω satisfying Eq. (11). The conditions could be divided into two parts: $\omega = 0$ and $\omega \neq 0$. When $\omega = 0$ there are not solutions of Eq. (8) for finite delays, yielding condition (ii) above. For all $\omega \geq 0$, we analyze the quadratic equation $(K_p - \omega^2)^2 + \omega^2(K_d + C)^2 - a^2 - (b\omega)^2 = 0$. When $K_p > \frac{1}{2}((K_d + C)^2 - b^2)$, the lowest point of quadratic equation is located in the right of plane; when $K_p < \frac{1}{2}((K_d + C)^2 - b^2)$, the lowest point of quadratic equation is located in the left of plane. Obviously, the inequality of $K_p > \frac{1}{2}((K_d + C)^2 - b^2)$ is satisfied because of $\omega^2 > 0$, and condition (iii) is satisfied considering Vieta theorem of quadratic equation. This completes the proof.

Now let us analyze the sufficient delay-independent stability region $(K_p, K_d + C)$. The inequalities listed in Theorem 5 are plotted and stability region is identified as shown in Fig. 5, where the boundary of condition (iii) is slope to the boundary of $K_p = a$ at point $(K_p, K_d + C) = (a, \sqrt{2a + b^2})$. The conditions of Theorem 6 can be seen to be equivalent to the three conditions above, in order to further reduce the difficulty of practical control design.

Theorem 6. *The input–output system defined by transfer Eq. (9) is stable independent of delays if the two conditions hold:*

(i) $K_p \geq a > 0$,
(ii) $K_d + C < \sqrt{2K_p + b^2}$

The red solid curves correspond to the boundaries defined by the inequalities in conditions (i), (ii) and (iii) of Theorem 5. The green curve determined by $K_d + C = \sqrt{2K_p + b^2}$ is shown to crystallize the boundary of condition (ii) of Theorem 6. The remaining blue dotted curves represent the necessary and sufficient conditions shown in Fig. 4 given here for comparison purposes. This completes the proof.

We conclude Theorems 5 and 6 in Fig. 5. A comparison is given in Fig. 5, where the necessary and sufficient conditions from Fig. 4 are also displayed. By comparison, the boundaries defining the sufficient stability conditions do not intersect with the curves related to the necessary and sufficient conditions, meanwhile, stability region associated with sufficient conditions is smaller than that with necessary and sufficient conditions. However, an analytical solution of necessary and sufficient conditions does not exist because it is difficult to deal with the trigonometric functions in Eqs. (14) and (15). So, it is easy to design the controller of system (8) according to Theorem 6.

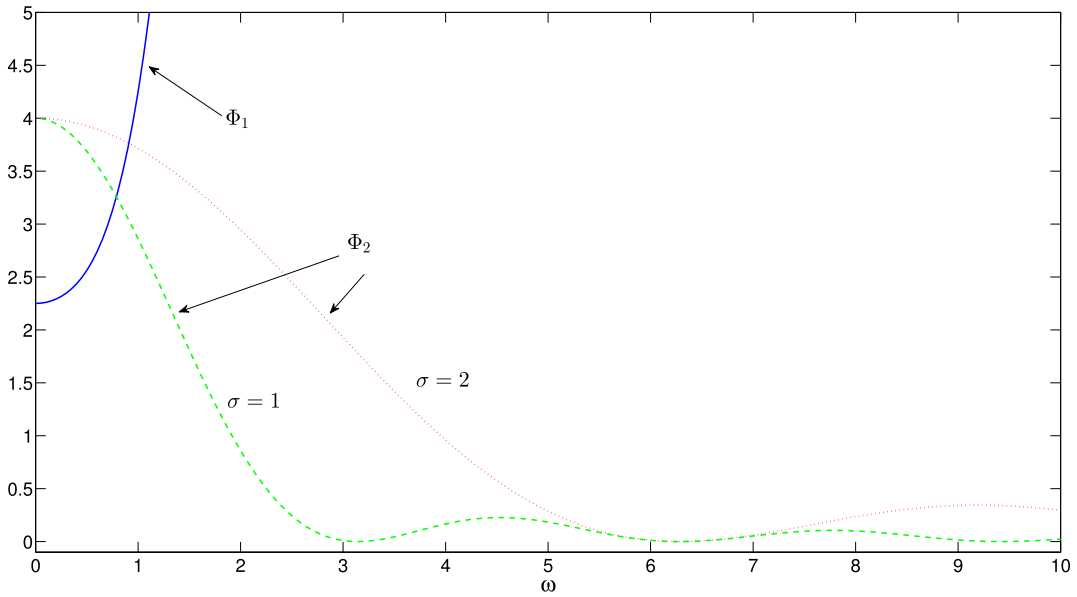

Fig. 6. The common solutions are the intersection points of between Φ_1 and Φ_2.

3.4. Stability of delay parameters of memory effect

In this section, we will attempt to reveal stability region considering delays (θ, σ), given gains K_p and $K_d + C$. However, stability analysis considering delays (θ, σ) needs further effort since the equations are presented by implicit forms and requires the solution of explicit functions.

In order to address the solutions of θ and σ from the characteristic Eq. (9), we restart to operate Eq. (18). By means of algebraic manipulations, we obtain the following formula:

$$(K_p - \omega^2)^2 + \omega^2(K_d + C)^2 = (a^2 + (b\omega)^2)\frac{2[1 - \cos(\omega\sigma)]}{(\omega\sigma)^2}, \tag{20}$$

The right side of Eq. (20) is seen as known entity for a given $\lambda = \sigma\omega$. We sweep $\lambda \in R^+$ and solve for ω as a function of the remaining parameters. Due to the fourth-order form of Eq. (20), the four ω roots can be solved analytically, and positive real roots are selected among these roots. One can compute σ via the relation $\sigma = \lambda/\omega$. Adopting combination method of algebra and geometry, we let $\Phi_1 = (K_p - \omega^2)^2 + \omega^2(K_d + C)^2$ and $\Phi_2 = (a^2 + (b\omega)^2)\frac{2[1-\cos(\omega\sigma)]}{(\omega\sigma)^2}$. Meanwhile, we look for the common solutions, that is, the intersection points between the curves of Φ_1 and Φ_2(Fig. 6).

In Fig. 6, blue line corresponds to Φ_1, green dash line corresponds to Φ_2 when $\sigma = 1$, and red dot line corresponds to Φ_2 when $\sigma = 2$. Once σ and ω is given, the relationship of θ satisfies the phase conditions obtained from Eqs. (11), (14) and (16).

$$\theta = -\frac{\sigma}{2} + \frac{1}{\omega}\left\{\arctan\left[\frac{[a(K_d + C) + b(\omega^2 - K_p)]\omega}{a(\omega^2 - K_p) + b\omega^2(K_d + C)}\right] + 2\pi k\right\}, k = 0, 1, 2, \ldots, \tag{21}$$

According to the formulation of Eq. (21), there are infinite number solutions for given (ω, σ). But they meet periodic condition with periodicity $\frac{2\pi}{\omega}$. Since Eq. (20) is complex nonlinear relation, we cannot be solved directly. However, we could study stability regions and controller gains considering delays (θ, σ) in the next.

4. Numerical simulation

Three case studies that consider different conditions are presented in this section. We will reveal how stability is affected by the change of controller gains in the controlled vehicle dynamics, and how different driver aggressiveness coefficients and memory delays are related to controller gains.

4.1. Controller gains space

Firstly, we analyze the gain parameter space $(K_p, K_d + C)$. Based on Theorem 2, we find stability boundary and stability region as shown in Fig. 5. Fig. 5 could be considered as the elaborate version of Fig. 4. The vertical boundary represents one

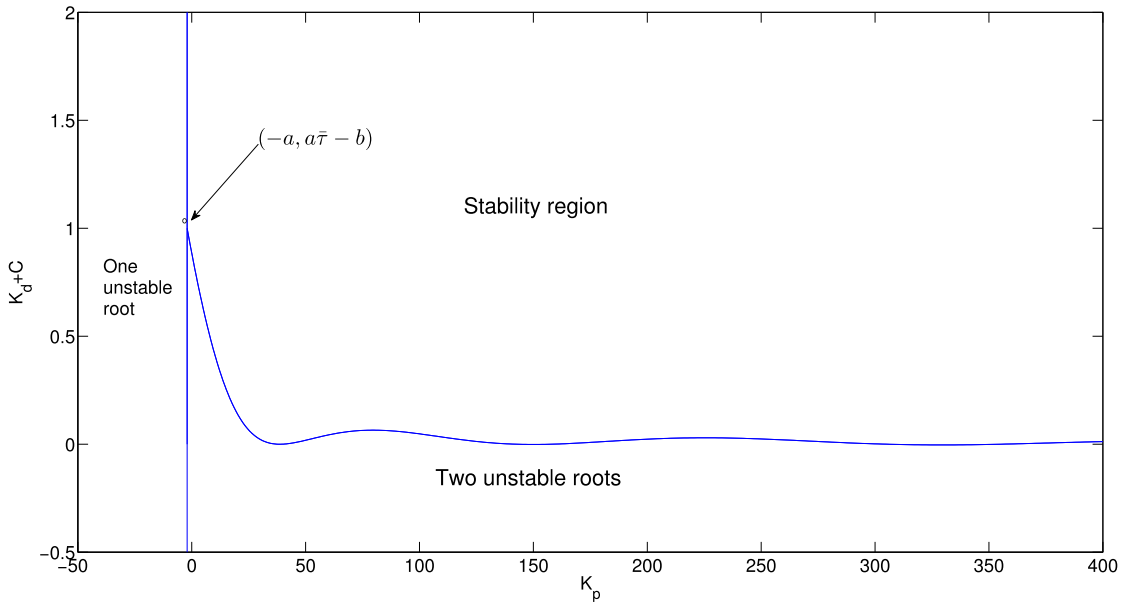

Fig. 7. Stability region of Theorem 2 considering two conditions.

Table 1
The algorithm process.

Algorithm
Initialization
Each λ starts from zero, and adds up to large upper bound L;
for i=1 to N do
Increase λ by small steps $\Delta\lambda = L/N$;
Compute the right-hand side of eq. (17) and solve ω,
If each ω meets $\omega \in R^+$ then
Find $\delta \in R^+$ via the formula $\sigma = \lambda/\omega$,
Find $\theta \geq 0$ from (18) for $k = 0, 1, 2, \ldots, K$, using σ and ω,
End if
End for

characteristic root residing at $s = 0$, and the remaining boundary corresponds to two characteristic roots ($s = j\omega, \omega > 0$) in the characteristic equation. The number of unstable roots can be identified in Fig. 7.

We clearly verify the analytical results we derived in the previous section. Particularly, we observe that sufficiently large combinations made up of K_p and $K_d + C$ make the vehicle dynamics stable. In Fig. 7, it is obvious that relatively larger K_p gains are needed to stabilize the vehicle dynamics compared with the magnitudes of the damping terms $K_d + C$. Moreover, a simple stability criterion can be formulated from Theorem 6. For example, let $K_p = 3 > a = 2$, then $K_d + C < \sqrt{6.04}$ guarantees delay-independent stability of the closed-loop system that contributes to designing the controller.

4.2. Driver's aggressiveness

Next, we study how driver's aggressiveness a and b affects stability regions. For this objective, we vary a or b to find stability boundaries. The results are shown in Figs. 8 and 9, where the stable region is shown by different curves to avoid confusion. In Fig. 8, when b is constant, increase of a could lead to shrinking some parts of stability regions. However, in Fig. 9, when a is constant, increase of b could lead to enlarging some parts of stability regions. We find that aggressiveness a and b go toward different direction.

4.3. Driver's memory effect

We are interested in stability region affected by delays (θ, σ) for controller gains and driver's aggressiveness given. The gains are chosen as $K_p = 2$ and $K_d + C = 1.5$. Driver's aggressiveness is taken as $a = 2, b = 0.2$. Based on Eq. (18), stability regions are computed, leading to Fig. 10. See Table 1 for specific algorithm.

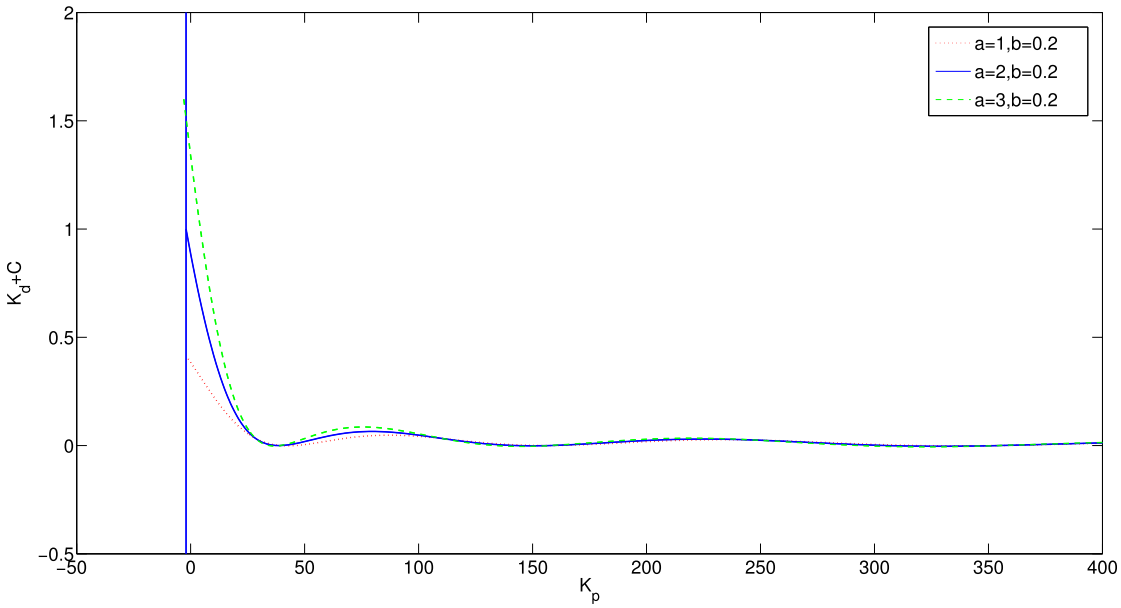

Fig. 8. Effect of a on stability regions when b is constant.

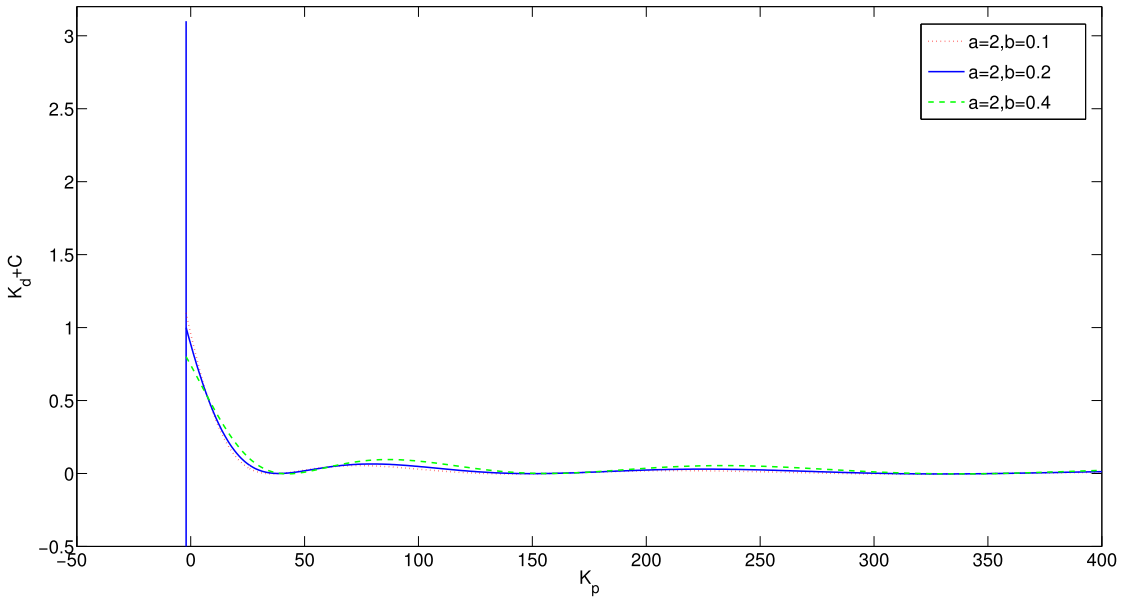

Fig. 9. Effect of b on stability regions when a is constant.

Fig. 10 shows stability region of delay parameters (θ, σ) about memory effect. Interestingly, the relationship between of dead time and memory window is depicted via triangle region. Moreover, we could observe that they are inverse proportion in upside of triangle. We consider larger dead-time θ is consumed for by reducing memory window σ when driver makes decision. In other words, detrimental effects that are brought by a large dead-time θ can be eliminated by a large memory size and controllers.

5. Conclusions

We present a new car-following model accounting for driver's characteristics and automation. The driver's memory effects are modeled with uniform distributions, while the automated controller is seen as PD controller without delay. We investigate stability of model dynamics that vehicles drive in single lane without changing lanes and overtaking.

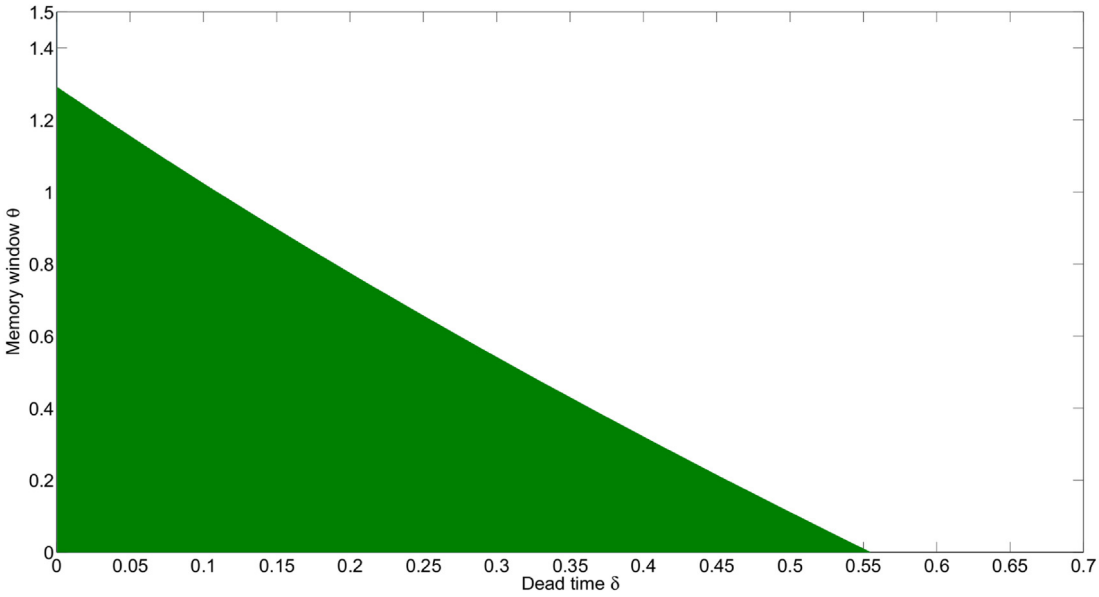

Fig. 10. Stability region of delay parameters (θ, σ).

Appropriate frequency-domain method is adopted to prove stability and reveal the inherent features of proposed model between driver's characteristics and automation. These studies demonstrate controller gains, driver aggressiveness and delays to linear stability of the controlled vehicle dynamics, and reveal the mathematic relation of those arguments. Some numerical examples are given to illustrate the effectiveness of the proposed methods and interpret the relation between driver's characteristics and automated controller, which obtains practical control design rules.

Acknowledgments

The authors gratefully acknowledge the research funding support from the National Natural Science Foundation of China (Grant No. 61803113), Guangxi Natural Science Foundation (Grant No. 2018GXNSFAA138036), Guangxi Natural Science Foundation (Grant No. 2016GXNSFAA380056), Guangxi science and technology base and special talent program (Grant No. Gui Ke AD18281015), Basic ability improvement project for young and middle-aged teachers in Guangxi universities (Grant No. 2018ky0201).

Conflicts of interest

The authors declare that there are no conflicts of interest regarding the publication of this paper.

References

[1] National Highway Traffic Safety Administration. Traffic Safety Facts 2013[J/OL]: https://crashstats.nhtsa.dot.gov/Api/Public/ViewPublication/812139.
[2] B. Soualmi, C. Sentouh, J.C. Popieul, S. Debernard, Automation-driver cooperative driving in presence of undetected obstacles, Control Eng. Pract. 24 (2014) 106–119.
[3] P.Y. Hsiao, C.W. Yeh, S.S. Huang, L.C. Fu, A portable vision-based real-time lane departure warning system: day and night, IEEE Trans. Veh. Technol. 58 (2009) 2089–2094.
[4] N.M. Enache, S. Mammar, M. Netto, B. Lusetti, Driver steering assistance for lane-departure avoidance based on hybrid automata and composite Lyapunov function, IEEE Trans. Intell. Transp. Syst. 17 (2010) 28–39.
[5] G.N. Bifulco, L. Pariota, F. Simonelli, Development and testing of a fully adaptive cruise control system, Transp. Res. C 29 (2013) 156–170.
[6] M. Wang, W. Daamen, S.P. Hoogendoorn, B.V. Arem, Rolling horizon control framework for driver assistance systems, part ii: cooperative sensing and cooperative control, Transp. Res. C 40 (2014) 290–311.
[7] K.C. Dey, L. Yan, X. Wang, Y. Wang, A review of communication, driver characteristics, and controls aspects of cooperative adaptive cruise control, IEEE Trans. Intell. Transp. Syst. 17 (2015) 1–19.
[8] M. Mulder, D.A. Abbink, E.R. Boer, Sharing control with haptics seamless driver support from manual to automatic control, Hum. Factors 54 (2012) 786–798.
[9] F. Flemisch, M. Heesen, T. Hesse, J. Kelsch, A. Schieben, J. Beller, Towards a dynamic balance between humans and automation: authority, ability, responsibility and control in shared and cooperative control situations, Cogn. Technol. Work 14 (2011) 3–18.
[10] L. Saleh, P. Chevrel, F. Claveau, J.F. Lafay, F. Mars, Shared steering control between a driver and an automation: stability in the presence of driver behavior uncertainty, IEEE Trans. Intell. Transp. Syst. 14 (2013) 974–983.

[11] B. Soualmi, C. Sentouh, J.C. Popieul, S. Debernard, Automation-driver cooperative driving in presence of undetected obstacles, Control Eng. Pract. 24 (2014) 106–119.
[12] K. Konishi, H. Kokame, K. Hirata, Decentralized delayed-feedback control of an optimal velocity traffic model, Eur. Phys. J. B 15 (2000) 715–722.
[13] Y. Zheng, S.B. Li, J. Wang, D.P. Cao, K.Q. Li, Stability and scalability of homogeneous vehicular platoon: Study on the influence of information flow topologies, IEEE Trans. Intell. Transp. Syst. 17 (2016) 14–26.
[14] D. Chen, D.H. Sun, M. Zhao, L.Y. Yang, T. Zhou, F. Xie, Distributed robust h∞ control of connected eco-driving system with time-varying delay and external disturbances in the vicinity of traffic signals, Nonlinear Dynam. 92 (2018) 1829–1844.
[15] L.C. Davis, Effect of adaptive cruise control systems on traffic flow, Phys. Rev. E 69 (2004) 066110.
[16] S.K. Li, L. Yang, Z.Y. Gao, K. Li, Stabilization strategies of a general nonlinear car-following model with varying reaction-time delay of the drivers, ISA Trans. 53 (2014) 1739–1745.
[17] S. Sheikholeslam, C.A. Desoer, Control of interconnected nonlinear dynamical systems: the platoon problem, IEEE Trans. Automat. Control 37 (1992) 806–810.
[18] H. Liu, D.H. Sun, M. Zhao, Analysis of traffic flow based on car-following theory: a cyber-physical perspective, Nonlinear Dynam. 84 (2016) 881–893.
[19] R. Sipahi, F.M. Atay, S.I. Niculescu, Stability of traffic flow with distributed delays modeling the memory effects of the drivers, J. Appl. Math. 68 (2007) 738–759.
[20] R. Sipahi, S.I. Niculescu, Stability of car following with human memory effects and automatic headway compensation, Philos. Trans. R. Soc. A 368 (2010) 4563–4583.
[21] P. Seiler, A. Pant, K. Hedrick, Disturbance propagation in vehicle strings, IEEE Trans. Automat. Control 49 (2004) 1835–1842.
[22] R. Rajamani, S.B. Choi, B.K. Law, J.K. Hedrick, R. Prohaska, P. Kretz, Design and experimental implementation of longitudinal control for a platoon of automated vehicles, J. Dyn. Syst. Meas. Control 122 (2000) 682–684.
[23] H. Hao, P. Barooah, Stability and robustness of large platoons of vehicles with double-integrator models and nearest neighbor interaction, Internat. J. Robust Nonlinear Control 23 (2013) 2097–2122.
[24] G. Orosz, R.E. Wilson, G. Stépán, Traffic jams: dynamics and control, Philos. Trans. R. Soc. A 368 (2010) 4455–4479.
[25] D. Chen, D.H. Sun, M. Zhao, Y.C. He, H. Liu, Weakly nonlinear analysis for car-following model with consideration of cooperation and time delays, Modern Phys. Lett. B 32 (2018) 1850241.
[26] T.Q. Tang, W.F. Shi, H.Y. Shang, Y.P. Wang, An extended car-following model with consideration of the reliability of inter-vehicle communication, Measurement 58 (2014) 286–293.
[27] S.W. Yu, Q.L. Liu, X.H. Li, Full velocity difference and acceleration model for a car-following theory, Commun. Nonlinear Sci. Numer. Simul. 18 (2013) 1229–1234.
[28] G.H. Peng, W.Z. Lu, H.D. He, Z. Gu, Nonlinear analysis of a new car-following model accounting for the optimal velocity changes with memory, Commun. Nonlinear Sci. Numer. Simul. 40 (2016) 197–205.
[29] J. Zhang, T.Q. Tang, S.W. Yu, An improved car-following model accounting for the preceding car's taillight, Physica A 492 (2018) 1831–1837.
[30] T.Q. Tang, Z.Y. Yi, J. Zhang, T. Wang, J.Q. Leng, A speed guidance strategy for multiple signalized intersections based on car-following model, Physica A 496 (2018) 399–409.
[31] W.X. Zhu, J. Du, L.D. Zhang, A compound compensation method for car-following model, Commun. Nonlinear Sci. Numer. Simul. 39 (2016) 427–441.
[32] D.H. Sun, D. Chen, M. Zhao, W.N. Liu, L.J. Zheng, Linear stability and nonlinear analyses of traffic waves for the general nonlinear car-following model with multi-time delays, Physica A 501 (2018) 293–307.
[33] S.W. Yu, Z.K. Shi, An improved car-following model considering relative velocity fluctuation, Commun. Nonlinear Sci. Numer. Simul. 36 (2016) 319–326.
[34] D. Ngoduy, Linear stability of a generalized multi-anticipative car following model with time delays, Commun. Nonlinear Sci. Numer. Simul. 22 (2015) 420–426.
[35] Q. Xin, N. Yang, R. Fu, S.W. Yu, Z.K. Shi, Impacts analysis of car following models considering variable vehicular gap policies, Physica A 501 (2018) 338–355.
[36] J. Zhang, T.Q. Tang, S.W. Yu, An improved car-following model accounting for the preceding car's taillight, Physica A 492 (2018) 1831–1837.
[37] S.W. Yu, J.J. Tang, Q. Xin, Relative velocity difference model for the car-following theory, Nonlinear Dynam. 91 (2017) 1–14.
[38] H. Kuang, Z.P. Xu, X.L. Li, S.M. Lo, An extended car-following model accounting for the average headway effect in intelligent transportation system, Physica A 471 (2017) 778–787.
[39] S.W. Yu, Z.K. Shi, Dynamics of connected cruise control systems considering velocity changes with memory feedback, Measurement 64 (2015) 34–48.
[40] S.W. Yu, Z.K. Shi, An extended car-following model considering vehicular gap fluctuation, Measurement 70 (2015) 137–147.
[41] T.Q. Tang, C.Y. Li, H.J. Huang, H.Y. Shang, A new fundamental diagram theory with the individual difference of the driver's perception ability, Nonlinear Dynam. 67 (2012) 2255–2265.
[42] He, S.C. Yang, H.Y. Shang, A car-following model accounting for the driver's attribution, Physica A 413 (2014) 583–591.
[43] T.Q. Tang, H.J. Huang, H.Y. Shang, An extended macro traffic flow model accounting for the driver's bounded rationality and numerical tests, Physica A 468 (2017) 322–333.
[44] H. Ou, T.Q. Tang, J. Zhang, J.M. Zhou, A car-following model accounting for probability distribution, Physica A 505 (2018) 105–113.
[45] L.A. Pipes, An operational analysis of traffic dynamics, J. Appl. Phys. 24 (1953) 274–281.